Received: 2 April 2019 | Revised: 17 April 2020 | Accepted: 1 July 2020

DOI: 10.1111/jfr3.12657

ORIGINAL ARTICLE

CIWEM Chartered Institution of Water and Environmental Management | Journal of Flood Risk Management | WILEY

# Hydrodynamic effect on non-stationary vehicles at varying Froude numbers under subcritical flows on flat roadways

**Syed Muzzamil Hussain Shah**[1] | **Zahiraniza Mustaffa**[2] | **Eduardo Matínez-Gomariz**[3] | **Khamaruzaman Wan Yusof**[2]

[1]Civil Engineering Department, Sir Syed University of Engineering and Technology, Karachi, Pakistan

[2]Department of Civil and Environmental Engineering, Universiti Teknologi PETRONAS, Seri Iskandar, Perak, Malaysia

[3]Department of Civil and Environmental Engineering, FLUMEN Research Institute, Technical University of Catalonia, Barcelona, Spain

**Correspondence**
Syed Muzzamil Hussain Shah, Civil Engineering Department, Sir Syed University of Engineering and Technology, 75300 Karachi, Pakistan.
Email: drmuzzamil@ssuet.edu.pk

**Funding information**
Technology Innovation Program funded by the Ministry of Trade, Industry & Energy (MI, Korea), Grant/Award Number: 10053121; Universiti Teknologi PETRONAS (UTP) Internal Grant, Grant/Award Number: URIF 0153AAG24

**Abstract**

Water is essentially a powerful component, strong enough to even move vehicles at the lowest hydraulic parameters. The flow orientation as well as the geometric and physical characteristics of a vehicle attribute to the way floodwaters affect and control the vehicle. Herein an effort has been made to study the hydrodynamic impact on a non-stationary vehicle partially submerged attempting to cross a flooded roadway (flat conditions). In arriving at the outcomes, extensive experimental testing was carried out on a Malaysian made city car, Perodua Viva (1:10), which was controlled to be partially submerged under the influence of subcritical flows. The experimental data was proven through theoretical equations based on the instability failure modes. The variation of the Froude number with respect to varying hydrodynamic forces has been further explored and conversed. The incipient velocity formulation proposed herein has been validated through the experimental data and the results showed good agreement between the two with a correlation coefficient of $R^2 = 0.85$. Among the main findings, it was noticed that the buoyancy force governed vehicle weight at depths greater than and equal to 0.0457 m for the scaled model. On the other hand, below critical depth, the dominancy of the drag force over frictional resistance and driving force caused sliding instability.

**KEYWORDS**

flat roadways, floods, Froude number, hydrodynamic forces, non-stationary vehicle, partial submergence

## 1 | INTRODUCTION

Hazards related to the vehicles exposed to floodwaters are based on the determination of their instability thresholds assessed from the hydraulic variables that is, flow water depth and velocity (Russo, Velasco, & Suñer, 2013; Sanyal & Lu, 2006; Smith, Modra, & Felder, 2019; Van Drie, Simon, & Schymitzek, 2008). A vehicle's stability would be compromised when the hydraulic variables exceed a certain limit, when exposed to flood flows (Abt, Wittier, Taylor, & Love, 1989; Russo, Gómez, & Macchione, 2013; Xia, Falconer, Wang, & Xiao, 2014). In the case of vehicles, characteristics like weight, chassis design, ground clearance and sealing capacity determines the level of stability (Martínez-Gomariz, Gómez, Russo, Sánchez, & Montes, 2019). Existing design guidelines are

based on the product of flow depth and velocity obtained during the experimental investigations performed on stationary vehicles in the late 1960's (Bonham & Hattersley, 1967) and early 1970's (Gordon & Stone, 1973); and the theoretical analysis assessed in the early 1990's (Keller & Mitsch, 1993). It has been established that there was no significant research published in the field of vehicle stability after the theoretical analyses carried by Keller and Mitsch (1993) until 2010. Therefore, the existing and up to date safety guidelines proposed in the Australian Rainfall and Runoff (AR&R) guidelines on vehicle stability in floodwaters are based on the hydraulic variables proposed in the earlier investigations (1967–1993), particularly for stationary vehicles (Shand, Cox, Blacka, & Smith, 2011).

Note that car designs and roadway conditions evolved towards improvement with time, thus variety of vehicle dimensions have been tested in recent years to further explore the instability criteria of modern cars in floodwaters. This involves the work of (Martínez-Gomariz, Gómez, Russo, & Djordjevi c, 2017; Shu, Xia, Falconer, & Lin, 2011; Teo, 2010; Toda, Ishigaki, & Ozaki, 2013; Xia, Falconer, Xiao, & Wang, 2013; Xia, Teo, Lin, & Falconer, 2010). However, all reported studies so far have been solely dedicated to static vehicles. Therefore, it is believed that considering vehicles in motion endangered by floodwaters needs attention.

The impact of hydrodynamic forces, namely friction, drag, buoyancy and lift forces pertaining to static vehicles (parked) have been discussed in detail in the former studies (Martínez-Gomariz, Gómez, Russo, & Djordjevi c, 2016; Martínez-Gomariz et al., 2019; Shu et al., 2011; Shah, Mustaffa, & Yusof, 2018; Shah, Mustaffa, Yusof, & Nor, 2018; Teo, Falconer, & Lin, 2012; Teo, Falconer, Lin, & Xia, 2012; Xia et al., 2010). Due to applied braking conditions, the frictional force on the static vehicles mainly focuses on the static friction coefficient. However, when it comes to instability mechanisms of a non-stationary vehicle, several parameters including the type of friction between the tires and the ground surface differs. For instance, when a vehicle attempts to cross a flooded street (*perpendicular to the flow direction*), the impact of friction acts in two directions, namely on the tires in the perpendicular direction of the incoming flow and secondly, due to tire rotation in the direction of vehicle movement. In the current investigation, the friction coefficients for both directions were experimentally determined. In addition to this, a supplementary force caused by vehicle engine, also known as the driving force, has also been introduced which opposes the drag force caused by the incoming flow. Moreover, for the given circumstances, the drag force does not only affect the side end of the vehicle facing the flow direction but also at the front vehicle chassis area intersecting with the floodwater. On the other hand, the impact of the vertical uplift force, namely buoyancy and lift force to cause floating instability failure remains the same as per past descriptions and assumptions. These issues have been brought up in this study which are further discussed in latter sections ensuring that the water levels were set in close resemblance to the limits allowed in terms of the height of car (partial submergence). Moreover, the range of flow velocities and depths ensured that the flow was subcritical.

## 2 | HYDRODYNAMIC FORCES

Moving water, particularly floodwaters, can cause a vehicle to float, slide or roll on urban floodplains. An understanding of the relevant forces involved in this phenomenon is necessary to characterise the instability thresholds of vehicles in floodwater flows subjected to frictional resistance ($F_R$), rolling friction ($F_{RO}$), the normal reaction force from the ground ($F_N$) which is equivalent to the net weight of the vehicle ($F_G$), the vertical uplift force ($F_V$) which is equivalent to the sum of the buoyancy ($F_B$) and lift force ($F_L$) the drag force perpendicular to the direction of the incoming, the drag force perpendicular to the direction of the incoming flow ($F_{D1}$), the drag force parallel to the direction of vehicle movement ($F_{D2}$) and the driving force caused by the vehicle engine ($F_{DV}$) as shown in Figure 1.

Experimental investigations pertaining to the assessment of hydrodynamic forces on static vehicles have been discussed in detail in former studies (Martínez-Gomariz

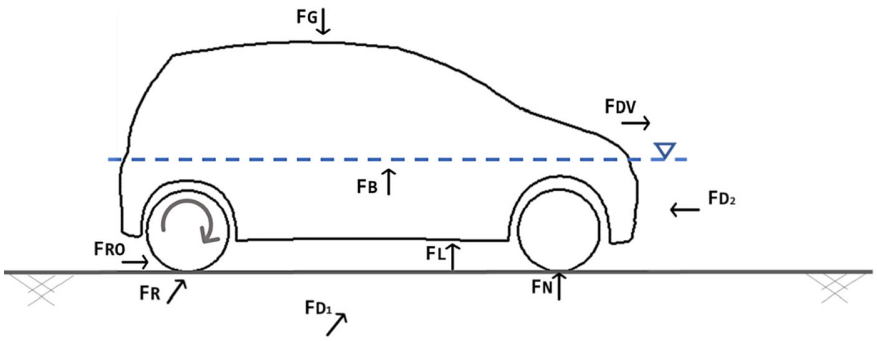


**FIGURE 1** Hydrodynamic forces on a non-stationary vehicle in floodwaters

et al., 2017; Shah, Mustaffa, Matínez-Gomariz, Kim, & Yusof, 2019; Shu et al., 2011; Teo, Falconer, & Lin, 2012; Teo, Falconer, Lin, & Xia, 2012; Xia et al., 2010). Although public safety is the primary aim of any flood risk management strategy, the numerical studies of vehicles' instability under water flow are sparse (Arrighi, Castelli, & Oumeraci, 2016). Herein attention was given to the vehicles in motion endangered by floodwaters, therefore the focus would be more on the rolling friction triggered due to tire rotation and the driving force produced by the vehicle engine. The rolling resistance can be simply defined as the energy a tire consumes while rolling under a given load. This resistance is influenced by the friction between the tire tread and the road surface, and the amount of energy consumed by flexing of the tire sidewalls as the tire rolls over the road as shown in Figure 2 (Ejsmont, Ronowski, Świeczko-Żurek, & Sommer, 2017). This scenario has been elaborated in further detail by summing up all the forces and dimensions separately, as shown in Figure 3. From the forces perspective, $F_{RO}$ is the force required to keep the wheel rolling, $W$ is the weight of the load, $R$ is the reactionary force and $\varnothing$ is the angle which relates to these three factors. From the pure dimensions point of view, r is the radius of the wheel and $b$ is the rolling coefficient which is measured in distance (Biezen, 2017).

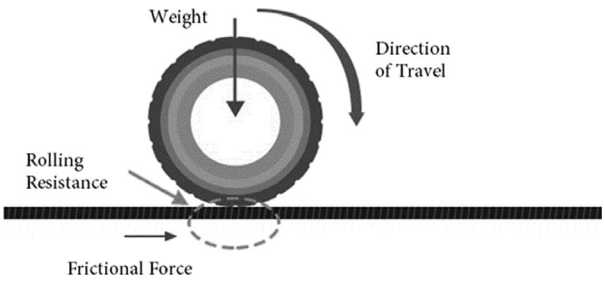


**FIGURE 2** Tire rolling resistance

From a force perspective, it can be assumed that:

$$R\sin\varnothing = F_{RO} \tag{1}$$

where, $R$ is the reaction force caused by the friction force, $\varnothing$ is the angle and $F_{RO}$ is the force required to keep the tire rolling. Following the concept of small-angle approximation, it can be assumed that $\sin\varnothing \approx \tan\varnothing \approx \varnothing$, therefore Equation (1) can be written as:

$$R\varnothing \approx F_{RO} \tag{2}$$

Through multiplication and division of the left-hand side of Equation (2) by the radius of the tire gives:

$$\frac{R\varnothing r}{r} = F_{RO} \tag{3}$$

From a pure dimensions point of view, it can be seen that $\sin\varnothing = \frac{b}{r}$, since $\sin\varnothing \approx \varnothing$ therefore, $\varnothing r \approx b$. Thus, substituting the value of $\varnothing r$ in Equation (3) gives:

$$\mathrm{Rb} \approx F_{RO}\, r \tag{4}$$

Through the use of Pythagoras theorem, the equation may be translated into,

$$R = \sqrt{W^2 + {F_{RO}}^2} \tag{5}$$

Squaring Equation (4) on both sides gives,

$$R^2 b^2 = {F_{RO}}^2 r^2 \tag{6}$$

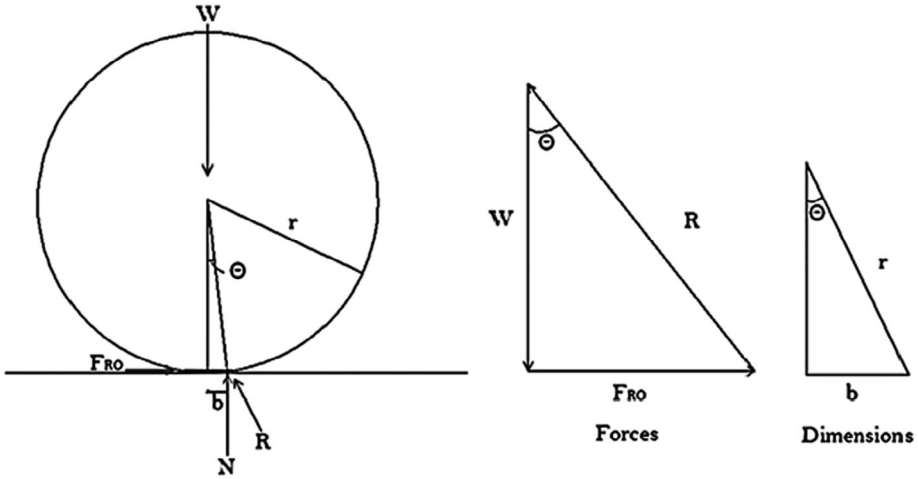


**FIGURE 3** Schematic diagram of forces and dimensions (Biezen, 2017)

Substituting for the parameter $R$ from Equation (5) into Equation (6), the equation becomes,

$$F_{\mathrm{RO}} = \frac{Wb}{\sqrt{r^2 - b^2}} \tag{7}$$

For vehicles in floodwaters where the state of the flow remains subcritical, the impact of the lift force has been reported as insignificant, thus Equation (7) can be re-written as:

$$F_{\mathrm{RO}} = \frac{(W - F_B) \cdot b}{\sqrt{r^2 - b^2}} \tag{8}$$

where, W is the weight of the load in dry conditions, b is the distance from the middle of the centre of the axle towards the tire, which no longer touching the ground, and r is the radius of the tire (Biezen, 2017).

The car engine provides the driving force when it just begins to move. This driving force is greater than the opposing force on the wheels. Therefore, the vehicle accelerates in the direction of the resultant force. Once moving, the vehicle moves through air column, which exerts a force on the car opposite to its direction. This force is called the air resistance, which increases with the speed of the car (Royston, 2013). In the current investigation, the impact of air resistance has been neglected due to low vehicle speed as it enter floodwaters, thus the impact of the flow resistance in the form of a drag force was taken into consideration. The driving force ($F_{\mathrm{DV}}$) caused by a vehicle engine can therefore be given as:

$$F_{\mathrm{DV}} = ma \tag{9}$$

where, m is the mass of the vehicle in floodwater and a is the average acceleration which can be given as:

$$a = \frac{v_f - v_o}{t} \tag{10}$$

where, $v_f$ is the final velocity, $v_o$ is the initial velocity and t is the time taken by the initial velocity to reach the final velocity. For vehicles moving at a constant velocity in floods, the net force acting on it becomes zero, thus the influence of driving force becomes negligible for this case. On flat roadways and in the absence of floods, the normal reaction force is equivalent to the vehicle weight, which can be written as:

$$F_N = W = mg \tag{11}$$

$$m = \frac{F_N}{g} \tag{12}$$

For studies performed in water, the net weight of the vehicle is equivalent to the vehicle weight in dry conditions, minus the vertical uplift force. However, for subcritical flow state, the net weight of the vehicle can be given as:

$$F_N = W - F_B \tag{13}$$

Substituting Equation (13) into Equation (12) gives:

$$m = \frac{W - F_B}{g} \tag{14}$$

Substituting Equation (14) into Equation (9), gives for the final equation:

$$F_{\mathrm{DV}} = \left(\frac{W - F_B}{g}\right) \times a \tag{15}$$

where, $g$ is the acceleration due to gravity and $a$ is the vehicle acceleration.

## 3 | METHODOLOGY

Experimental runs with the non-static model were carried out in a physical model of a water retaining structure ($5 \times 4.25\ \mathrm{m}^2$) located in the Hydraulics Laboratory, Universiti Teknologi PETRONAS (UTP), Malaysia. Note that the maximum capacity for the pond to hold the water depth was 0.35 m. While computing the hydraulic variables, that is, flood depth ($y$) and velocity ($v$), a hanging bridge connected to the ceiling was used to avoid direct contact with the flow. The measurement tools, such as a pointed gauge, current meter, camcorder and line laser, were placed on the moveable hanging bridge. The velocity and water depth measurements were observed at one vehicle length upstream of the flooded vehicle (Xia et al., 2010). Herein a moving Perodua Viva, which represents a typical sized Malaysian passenger car, was modelled ($\therefore \rho_p = \rho_m = 1$) at a scale of 1:10, following the conditions of similitude. The model was tested under varying discharges and water depth conditions, through which the instability was computed. The specifications of the model and prototype are shown in Table 1. The time taken by the vehicle to reach a known distance was also recorded for the estimation of driving force. The water levels were set in close resemblance to the limits allowed in terms of the height of car (partial submergence). Moreover, the range of flow velocities and depths ensured that the flow was subcritical. Keeping in mind the height of the car, the range of water depths tested was between 0.038 and 0.099 m, with flow

**TABLE 1** Perodua viva dimensions and specifications

| Vehicle | Scale | Length (mm) | Width (mm) | Height (mm) | Kerb weight (g) |
|---|---|---|---|---|---|
| Perodua viva | Prototype | 3,575 | 1,475 | 1,530 | ≈800,000 |
| | Model (1:10) | 357.5 | 147.5 | 153.0 | 880 |

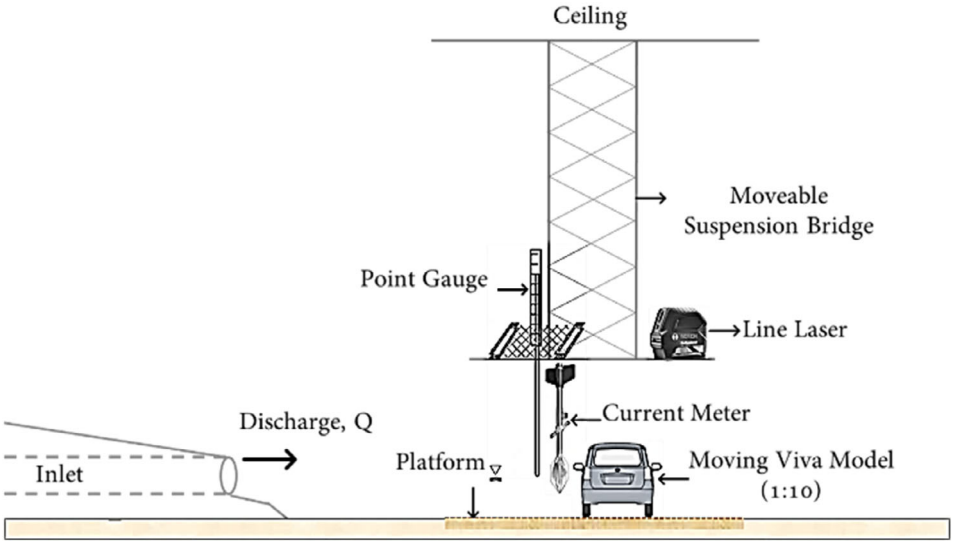


**FIGURE 4** Side view of experimental setup

velocities observed in the range of 0.18 to 0.61 m/s. Following similar steps, the experimental data were collected for several flow and depth combinations, to compute the vehicle's instability modes. The description and the schematic diagram of the experimental setup is shown in Figure 4.

A physical scale model is completely similar to its real-world prototype and involves no scale effects if it satisfies the following three criterions, namely geometric, kinematic and dynamic similarities. Geometric similarity requires similarity in shape which exists when all corresponding dimensions in model are $\lambda$ shorter than of its real-world prototype. For example, for a given scale ratio of 1:10, 1 represents the model dimension ($L_m$) which is 10 times shorter than of its prototype ($L_p$). This length scale ratio ($L_r$) can be given as:

$$L_r = \frac{L_p}{L_m} = \lambda \tag{16}$$

Similarly, flows in the flumes can be categorised as free surface flow which are generally driven both by gravity and inertia. Therefore, Froude number is the best correlation required to analyse the flow. The force ratio combination for Froude similarity can be given as:

$$\text{Froude number}\,(F) = \left(\frac{\text{Inertia Force}}{\text{Gravity Force}}\right)^{\frac{1}{2}} \tag{17}$$

$$\text{Froude number}\,(F) = \left(\frac{\rho L^2 v^2}{\rho V g}\right)^{\frac{1}{2}} \tag{18}$$

$$\text{Froude number}\,(F) = \frac{v}{\sqrt{gL}} \tag{19}$$

In terms of criterion both for model and prototype, the equation can be simplified to:

$$F_p = F_m \tag{20}$$

$$\frac{v_p}{\sqrt{gL_p}} = \frac{v_m}{\sqrt{gL_m}} \tag{21}$$

$$v_p = v_m (L_r)^{\frac{1}{2}} \tag{22}$$

where, $v$ is the velocity, $g$ is the gravitational force, and $L$ is the length scale. Subscripts $p$ and $m$ are for prototype and model, respectively.

## 4 | FLOW CHARACTERISTICS

The stability limits proposed by Moore and Power (2002) indicate that the buoyant force dominates instability when the floodwater depth is high and flow velocity is low. Similarly, the drag force dominates instability under

shallow water depths and high flows (Moore & Power, 2002). Herein a similar behaviour was witnessed while performing the experimental tests. Since the experiments were carried out under subcritical flow conditions, most of the threshold values were obtained at high water depths where the buoyancy force was dominant. The range of Froude numbers attained from the experimental investigations ensured the state of the flow as subcritical. The magnitude of the drag coefficient usually varies with the change of Reynolds number (*Re*) and it approaches a constant for large Reynolds numbers, that is, greater than 2000. The value of *Re* was assessed through the formula, $Re = Uh/\nu$, where "$U$" is the cross-sectional averaged velocity at the given flood depth "$h$" and "$\nu$" is the kinematic viscosity of water. Herein the minimum value of the Reynolds number was noticed to be in the order of 17,000, thus the drag coefficient was kept unchanged for the assessment of the drag force, both at $D_1$ and $D_2$.

## 5 | LABORATORY INVESTIGATIONS

The instability thresholds attained from the experimental investigations are highlighted in Figure 5. It was noticed that when the water depth was equal to, or greater than, 0.045 m, then floating instability failure was witnessed which probably happened due to the pressure exerted by the flood in the form of the vertical uplift force that exceeded the vehicle weight. Conversely, below this critical water depth, the mode of sliding instability was observed, based on the dominancy of the drag over friction and the driving forces. The instability thresholds attained from the experimental investigations were mainly based on visual observations. However, in the latter sections, the threshold values obtained by means of theoretical equations have been further assessed and compared with the laboratory investigations.

## 6 | COMPUTATION OF HYDRODYNAMIC FORCES

Herein the hydrodynamic forces which would lead to the possibility of floating and sliding instability failure have been theoretically assessed. In this regard, an innovative numerical approach has been proposed to determine the submerged fraction of the vehicle for different water depths. Furthermore, in the preceding studies relating to stationary flooded vehicles, the friction coefficient was usually set to a constant value ($\mu = 0.3$) as proposed by Bonham and Hattersley (1967), though it was later

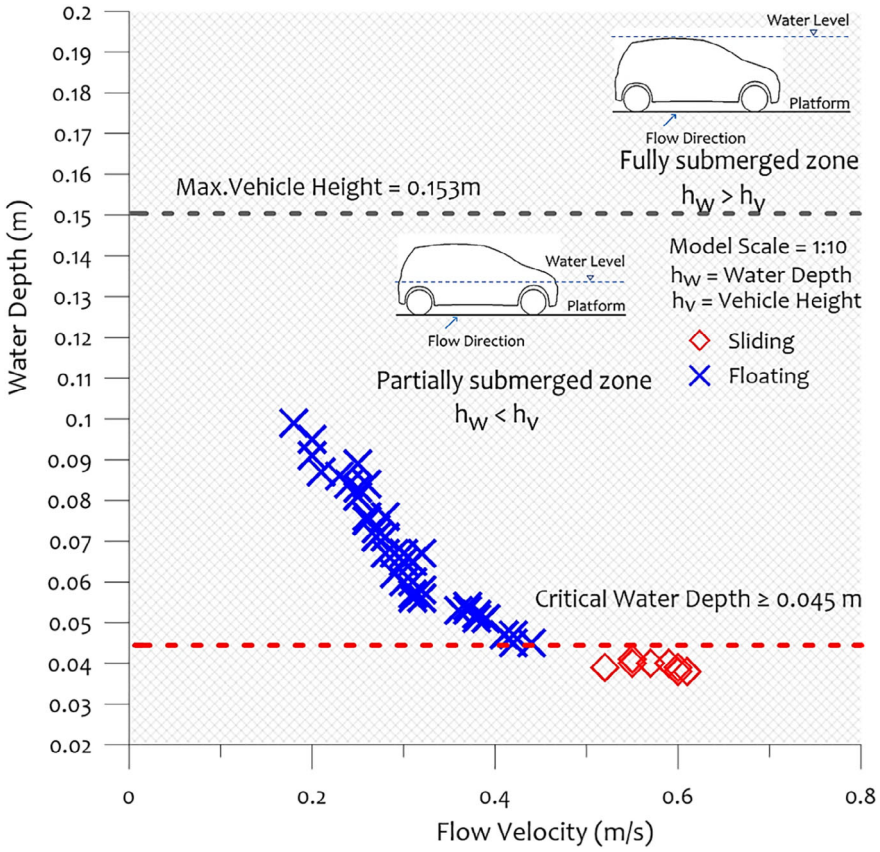


**FIGURE 5** Instability thresholds assessed through laboratory investigations

contradicted by Gordan and Stone (1973) ($\mu = 0.3$ to 1.0). However, in the existing study for non-stationary vehicles, the friction coefficients, both for frictional resistance μ and rolling resistance $\mu_{RO}$, were experimentally determined. On the other hand, the drag coefficient, $C_D$ was set to 1.1 or 1.15 depending on the depth of the floodwater with respect to the vehicle chassis. To the author's knowledge, a reliable assessment of drag and lift coefficients contributing to the incipient motion condition under different flow regimes needs to be conducted. Though today's computing capacities can carry out 3-dimensional numeric simulations on the drag and lift contribution to the incipient motion of partly submerged flooded vehicles, such studies are limited. More investigation of the force coefficients both for partial and full submergence is needed. It has been further shown that the effect of the vertical uplift force, which is equivalent to the sum of buoyancy and the lift force varies as based on the transition between the flow states. For instance, the impact of the buoyancy force can be neglected for high flow velocities, thereby considering only the effect of the lift force (Martínez-Gomariz et al., 2017). Herein the study was performed under subcritical flow conditions and for such flow regimes, the impact of the lift force has been reported insignificant (Shah, Mustaffa, Yusof, & Nor, 2018). Therefore, in the current investigation, the impact of the lift force has not been taken into consideration. Moreover, the Froude number relates to the gravity and inertia forces, a variation of the estimated forces with the Froude number has been individually discussed and presented in this study.

## 6.1 | Buoyancy force ($F_B$)

Recall that for the estimation of buoyancy force, the submerged volume ($V$), water density ($\rho$) and acceleration due to gravity ($g$) are required. Since $\rho$ and $g$ remain constant therefore, to attain the submerged volume of the vehicle at different water depths, the vehicle chassis and tires were drawn precisely. Initially, a 2D Model of the chassis and tires were separately designed and scaled to 1:10 through AutoCAD software, which was then extruded into a 3D Model by using Solid-Works software. Lastly, the volume of the water displaced by the vehicle chassis and the tires at varying water depths was obtained through the numerical tool ANSYS (Static Structural) as shown in Figure 6. The submerged volume of the body and tires was then used to estimate of buoyancy force for different water depths. However, the impact of the buoyancy force, with respect to the Froude number for different water depths, was noted and is presented in Figure 7.

It should be noted that the buoyancy force relies on the submerged volume of the immersed object, which varies with varying water depths. Herein, for every decrease in the water depth, an increase in the Froude number was recorded, because the Froude number is higher for larger velocities and lower water depths. For instance, at the lowest Froude number (0.18), the buoyancy force almost reached the maximum value of 33 N, whereas its effect was found to be insignificant at the high Froude number (0.98). Therefore, the above graph figured an inverse variation between the two.

## 6.2 | Drag force ($F_D$)

For parked vehicles, the horizontal force is mainly created by the drag force as it acts only in one direction, whereas the force that resist its impact in the opposite direction is the frictional force. Conversely, these measures differ when a non-stationary vehicle attempts to enter floods. In the current investigation, the direction of

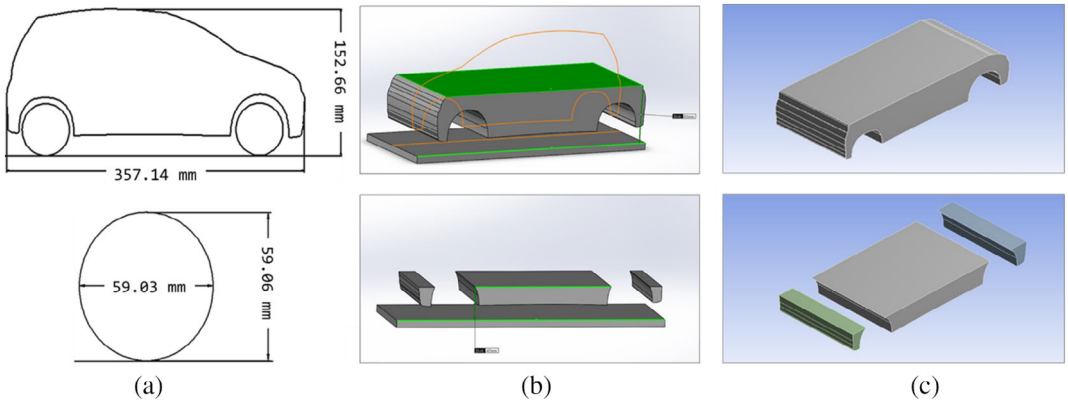


**FIGURE 6** Numerical modelling to assess a vehicle's submerged fractions: (a) AutoCAD, (b) Solid-Works and (c) ANSYS (Static Structural)

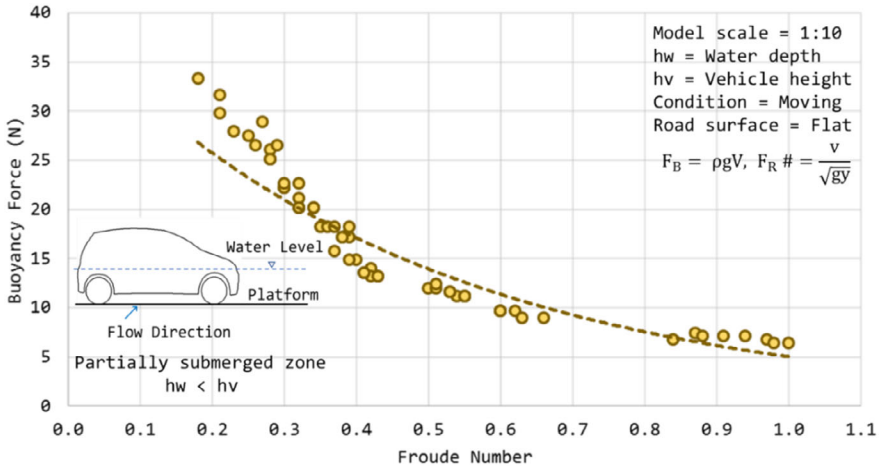


**FIGURE 7** Buoyancy force response at varying Froude numbers

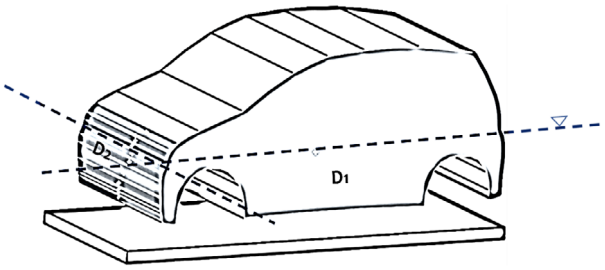


**FIGURE 8** Drag influence at side ($D_1$) and front end ($D_2$) of the vehicle

the flood flow was always perpendicular to the vehicle movement, therefore, under such circumstances, the vehicle's submerged area projected normal to the incoming flow ($D_1$) was mainly affected. Additionally, the drag force slightly affected the frontal bonnet area ($D_2$), as shown in Figure 8. On a similar note, the principles of friction force for a non-stationary car attempting to cross such streets also differs. Likewise, the impact of drag at the side and front ends, the tires resistance towards the drag force is also a two-directional effect, which is further discussed in the latter section.

From a theoretical perspective, the submerged area at $D_1$ and $D_2$ was estimated when the submerged volume of the vehicle at the known water depth was normalised by the vehicle width and length, respectively. On the other hand, the impact of the drag force on the vehicle wheels was estimated separately. For instance, at $D_1$, only the submerged area of the two tires facing the incoming flow direction was considered. Similarly, at $D_2$, the submerged area of the frontal two tires was considered. At $D_2$, the submerged area of the tires was comparatively small, due to frontal bumper area which already covered the vehicle chassis. It is important to emphasise that herein only those data points have been discussed which were below the critical water depth, because below the critical depth, the drag effect was more dominant. Likewise, the effect of the buoyancy force with respect to the Froude number, a variation in the form of the drag force ($D_1$) relative to the Froude number has also been discussed as shown in Figure 9.

It can be observed that for all the data points, the buoyancy effect was dominant at high water depths and low flow velocities. In contrast, sliding failure was controlled by high velocities and low water depths. It is recalled herein that only those data points have been discussed which were below the critical water depth. Thus, it can be observed that the magnitude of the drag force slightly increases with an increase in the Froude number, mainly because of the higher velocities. However, the overall impact of the drag force at $D_1$ was found to be higher because of the incoming flow direction and the larger available area. Later, with an increment in the Froude number, the drag influence increased accordingly. For instance, the maximum drag force was noticed to be approximately 1.5 N, when the value of Froude number reached 0.98.

An attempt was made to further study the influence of the drag force in the direction parallel to the vehicle movement ($D_2$) which indicated the flow strength on the vehicle in the opposite direction to that of the incoming flow. At $D_2$, the estimated flow velocity was found to be very low and nearly constant throughout, as it was opposing the main direction of the incoming flow. Moreover, the frontal part of the vehicle chassis provided a smaller submerged area compared to the side end. Therefore, the resultant drag force at $D_2$ was found to be nominal. Furthermore, due to a constant flow velocity, the drag force at $D_2$ mainly varied with the water depth. Thus, the drag influence in this direction increased with an increase in the water depth. Observations on the variation of the drag force ($D_2$) relative to Froude number are presented in Figure 10.

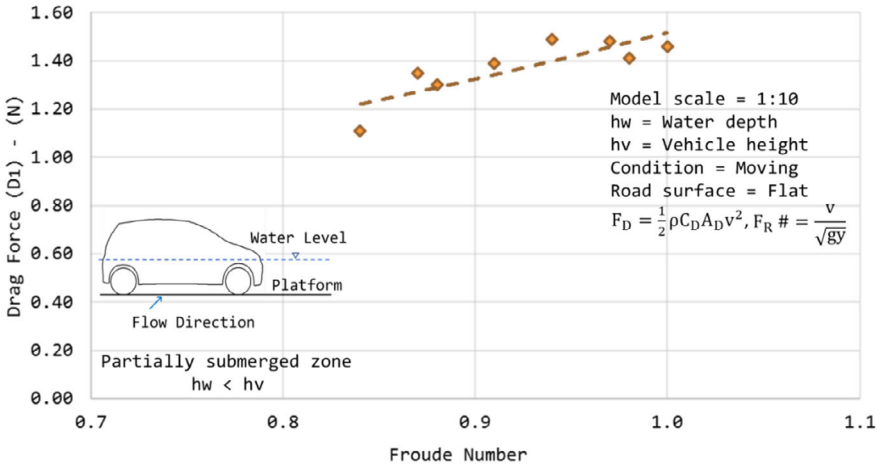


**FIGURE 9** Drag force ($D_1$) response at varying Froude numbers

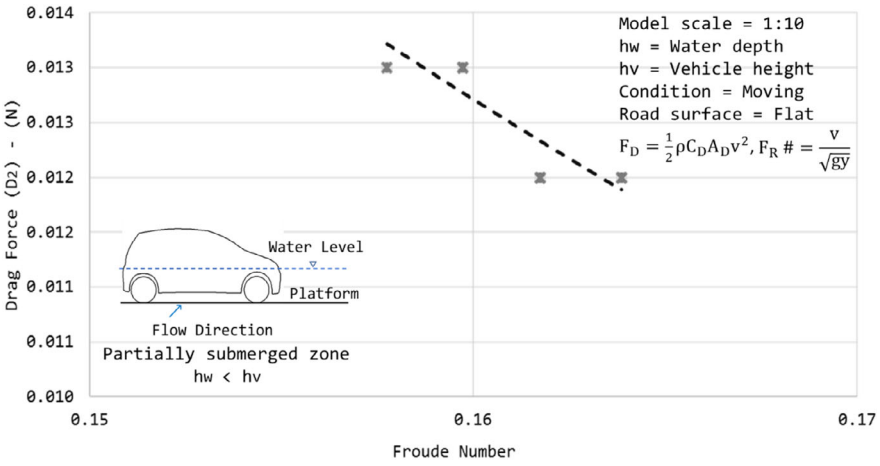


**FIGURE 10** Drag force ($D_2$) response at varying Froude numbers

From Figure 10, an inverse relationship was identified between the drag force and the Froude numbers. For a constant flow velocity of 0.01 m/s, the drag influence increased for every increment in the water depth which decreased the Froude number. Therefore, for the given circumstances that is, constant flow velocity, the Froude number was found to be inversely proportional to the square root of water depth and so does the drag force. For instance, when the Froude number reached a value of 0.158, the drag force was noticed to be 0.013 N. On the other hand, when the Froude number reached the value of 0.164, the impact of the drag force was found to be 0.012 N. Therefore, it can be said that the dependency of Froude number on the drag force varies with several parameters.

Upon comparing the impact of drag both at $D_1$ and $D_2$, it was noticed, that the maximum drag observed at $D_1$ was almost 1.5 N, whereas at $D_2$, it was only 0.012 N. Therefore, it can be summarised that the impact of the drag force for a partially submerged vehicle attempting to cross a subcritical flooded streets is mainly dominant in the direction of the incoming flow. This criterion could differ for the critical and super-critical flow conditions which should be investigated further in future. However, in the current investigation, the drag impact at $D_2$ has not been taken into consideration due to its nominal influence on the development of incipient velocity formula.

## 6.3 | Frictional resistance ($F_R$) and rolling friction ($F_{RO}$)

Under this section, the ability of a vehicle's tires to oppose sliding failure has been studied. A realistic value of surface roughness between the tires and the ground surface provides meaningful assessment of friction. In this regard, the Manning's coefficient of the designed platform was determined and was estimated to be 0.017. This figure nearly matches the Manning's coefficient for asphalt pavements, with a value for rough texture of 0.016 (Te-Chow, 1959). Likewise, the impact of the drag at the side and front ends, the ability of the vehicle to oppose sliding, is also generated in two directions,

namely $F_R$ and $F_{RO}$. Unlike the static friction coefficient, which is applicable to a stationary vehicle (brakes applied), the value of the friction coefficient for the non-stationary vehicle changes. Herein for the estimation of the friction force, the friction coefficients, namely $\mu$ and $\mu_{RO}$, were experimentally determined for the designed platform (i.e., wet conditions). The friction coefficient was estimated by applying the force manually through a spring balance. The friction force indicated on the spring balance, divided by the scale model weight, gave friction coefficient values both for $\mu$ and $\mu_{RO}$ (Martínez-Gomariz et al., 2017). For the flat roadway condition, the value of the friction coefficient parallel and opposite to the direction of the incoming flow was estimated to be 0.52, whereas its value in the direction of vehicle movement was found to 0.092.

In estimating the friction force, the effective weight of the vehicle, which is equivalent to the axle load under dry conditions minus the vertical uplift force, is required. Since in the current study the influence of buoyancy alone was assumed to be responsible for causing floating instability, the effective weight of the vehicle was obtained by deducting the buoyancy force from the vehicle weight under dry conditions. Likewise, the variation of the Froude number with respect to buoyancy and drag forces, its relation to $F_R$ and $F_{RO}$, was also studied and has been highlighted in Figures 11 and 12, respectively.

The friction force, $F_R$ is the resistive force which mainly acts in the parallel and opposite directions to the incoming flow, whereas the rolling friction, $F_{RO}$ is caused due to tires rotation in the direction of vehicle movement. It is important to emphasise that while estimating the effective weight of the vehicle for the assessment of the friction force, the buoyancy force is deducted from the vehicle's total weight. Although when the depth is below the critical water depth the impact of buoyancy force persists, but it is slightly less effective (i.e., insufficient to cause floating instability). For instance, consider the range of water depths in between the platform level and the critical water depth as shown in Figure 13. From the Figure, it can be perceived that when the water level would be at the platform level, the friction force would

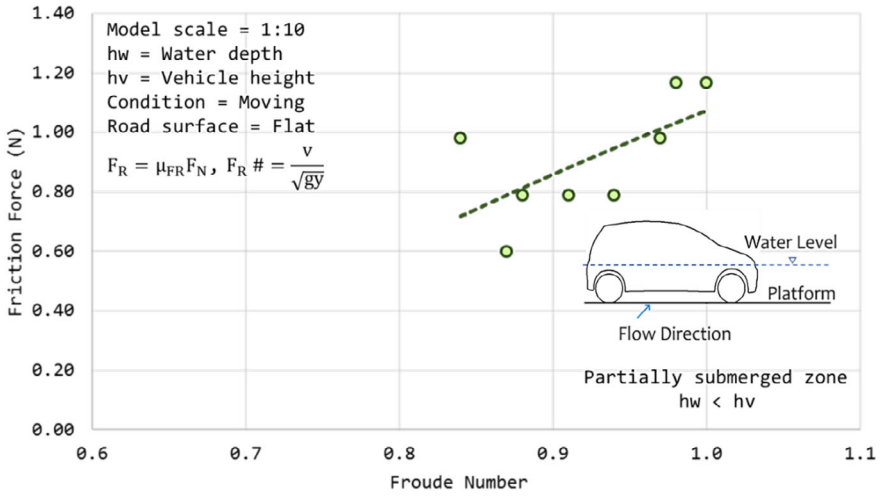


**FIGURE 11** Friction force, $F_R$ response at varying Froude numbers

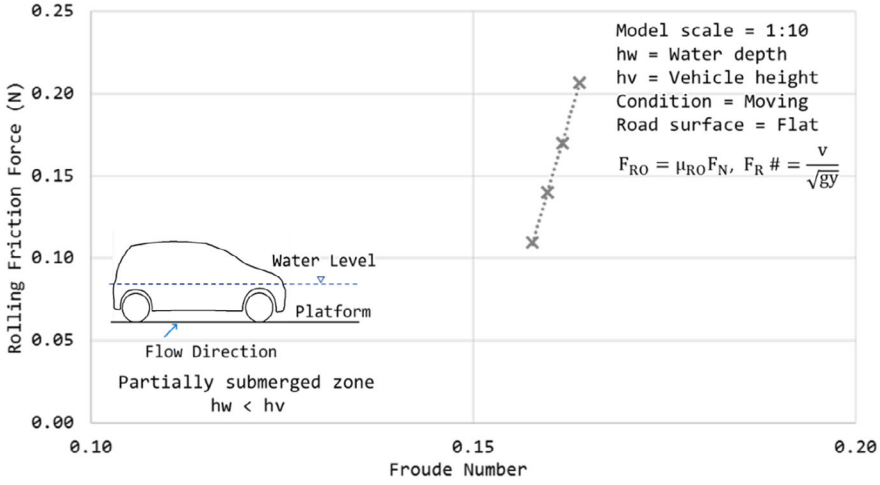


**FIGURE 12** Rolling friction force, $F_{RO}$ response at varying Froude numbers

be high due to the negligible impact of the buoyancy force. However, as the water level goes up, the impact of the buoyancy force would increase which, in turn, reduces the vehicle weight, and thus the contact of the tires with the ground is reduced. Therefore, it can be interpreted that at low Froude numbers, the chances of frictional stability of the vehicle with the ground is reduced and vice versa. Concerning $F_R$, it was noticed that when the Froude number reached the value of 0.83, the frictional resistance between the tire and the ground surface was minimal, whereas at higher Froude numbers, a maximum frictional resistance was noticed. On the other hand, the impact of $F_{RO}$ with respect to the Froude number followed the same criterion. For instance, at low Froude number, that is, 0.16, the influence of rolling friction was found to be minimal, whereas it was stronger at higher Froude numbers. Thus, it can be inferred that for any increment in the water depth, the influence of the frictional force (both $F_R$ and $F_{RO}$) on a non-stationary vehicle is reduced. Therefore, it is concluded that as the water depth around a vehicle vicinity increases, then the ability of a vehicle to stay in contact with the ground is reduced.

### 6.4 | Driving force ($F_{DV}$)

The car engine provides motion to the car which makes it accelerate in the forward direction. At high speeds, the vehicle forces the air out of the way, which exerts a force on the car in the opposite direction. This force is called the air resistance, which increases as the speed of the car increases (Royston, 2013). Herein a study was performed under controlled acceleration, that is, low velocities, to estimate the resistive force acting in the opposite direction to the driving force, which correspond to the drag force caused by the floodwater. The driving force was assessed by marking the points between two known distances on the designed platform. While performing the experiments, the time taken for a vehicle to cross the two known points was noted, thereby enabling on the estimation of the initial and final velocity of the car. The driving force caused by the vehicle's engine below the critical water depth is shown in Table 2.

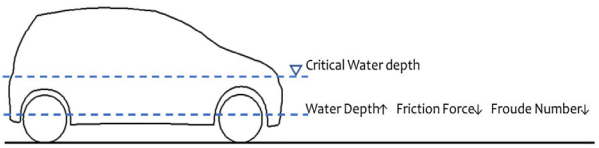


**FIGURE 13** Increment in the water depth and friction force

## 7 | COMPUTATION OF INSTABILITY FAILURE MODES

The manner in which the instability failure mechanism results for static vehicles has been well recognised in former studies. Herein the focus is more on the instability modes recognised by a non-stationary car attempting to cross a flat flooded roadway. With that regard, the vertical uplift force ($F_B$ and $F_L$) which would lead to the possibility of floating instability and the horizontal resultant force ($F_D$, $F_R$, $F_{RO}$, and $F_{DV}$) responsible for causing sliding were theoretically assessed. Since the study was performed for subcritical flow conditions, only the impact of buoyancy force was therefore taken into consideration, while computing the vertical uplift force. On the other hand, the impact of horizontal resultant force, namely the drag force, frictional resistance, rolling friction and driving forces were taken into account for the assessment of the sliding failure mechanism. Herein an incipient velocity formula based on the mechanical theory of

**TABLE 2** Driving force, $F_{DV}$

| No. | Distance (m), $D_1$ | Time (s), $T_1$ | Vehicle velocity (m/s), $V_1$ | Distance (m), $D_2$ | Time (s), $T_2$ | Vehicle velocity (m/s), $V_2$ | Acceleration ($m/s^2$) | Vehicle mass (kg) – Equation (14) | Driving force (N) – Equation (15) |
|---|---|---|---|---|---|---|---|---|---|
| 1. | 0.3048 | 1.97 | 0.15 | 0.6096 | 4.27 | 0.14 | 0.002 | 0.118 | 0.00023 |
| 7. | 0.3048 | 1.84 | 0.17 | 0.6096 | 4.69 | 0.13 | 0.005 | 0.155 | 0.00085 |
| 14. | 0.3048 | 1.04 | 0.29 | 0.6096 | 3.18 | 0.19 | 0.024 | 0.192 | 0.00461 |
| 20. | 0.3048 | 1.81 | 0.17 | 0.6096 | 4.61 | 0.13 | 0.006 | 0.155 | 0.00087 |
| 26. | 0.3048 | 1.61 | 0.19 | 0.6096 | 3.51 | 0.17 | 0.003 | 0.155 | 0.00047 |
| 27. | 0.3048 | 1.82 | 0.17 | 0.6096 | 3.99 | 0.15 | 0.003 | 0.192 | 0.00049 |
| 33. | 0.3048 | 1.34 | 0.23 | 0.6096 | 3.79 | 0.16 | 0.013 | 0.229 | 0.00297 |
| 53. | 0.3048 | 1.40 | 0.22 | 0.6096 | 3.15 | 0.19 | 0.005 | 0.229 | 0.00122 |

sliding equilibrium has been proposed for the non-stationary vehicle, which would be essential to determine the incipient velocity required to cause sliding failure if several parameters in the given equation are known.

Pertaining to non-stationary vehicles, the criterion for floating instability remains similar to the static cars specifically where the state of the flow remains subcritical. It may vary for other flow states, which would lead to the inclusion of the lift force for the assessment of vertical uplift force. However, floating instability is more influential at high water depths, where the velocity of the flow is usually moderate as shown in Figure 14. Thus, the mode of floating instability for a moving vehicle under the given circumstances can be expressed as:

$$F_B > W_T \tag{23}$$

where, $F_B$ is the buoyancy force and $W_T$ is vehicle weight in dry conditions.

When a non-stationary vehicle enters floodwaters (perpendicular to flow direction), the flow not only affects the side end projected normal to the flow, but also the front end of the vehicle, as it slowly progresses. Based on these assumptions, the impact of the drag force was analysed in two directions. The impact of the drag in both directions was separately estimated through a theoretical assessment. However, it was noticed that the effect of the drag at $D_1$ was higher due to the intensity of the incoming flow and the larger available area, whereas at $D_2$ it was found to be almost insignificant due to low flow velocity and the smaller frontal area. Thus, its impact to initiate sliding failure for the given situation was disregarded. Furthermore, being well familiar with the frictional force, its impact was also analysed in two directions by experimentally determining the friction coefficients for both cases, as highlighted in the former section. However, concerning the driving force, the impact of air drag was neglected due to low vehicle speed and thus, only the drag caused by floodwater flow was considered. On this basis, it has been proposed that the friction and the driving forces oppose the drag force to keep the vehicle stable. Thus, if the drag force exceeds the frictional and driving forces, then the possibility of a non-stationary car to slide along a flat roadway would increase as shown in Figure 15. Therefore, the principle equation to form sliding failure can be expressed as:

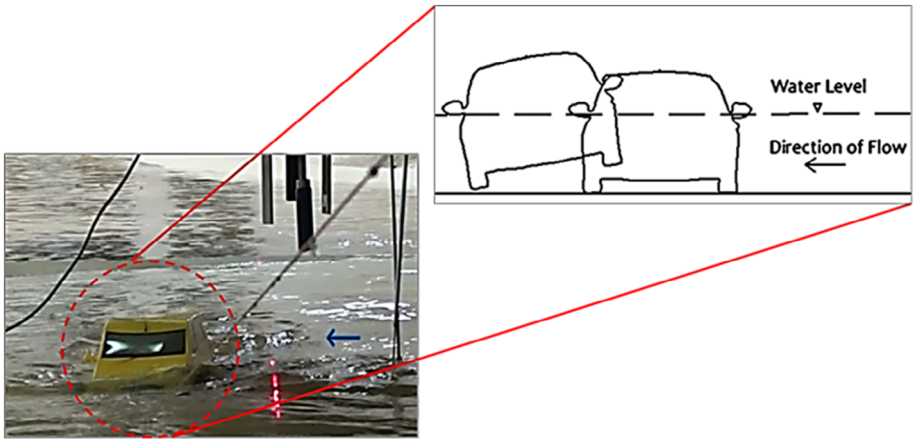


**FIGURE 14** Floating instability

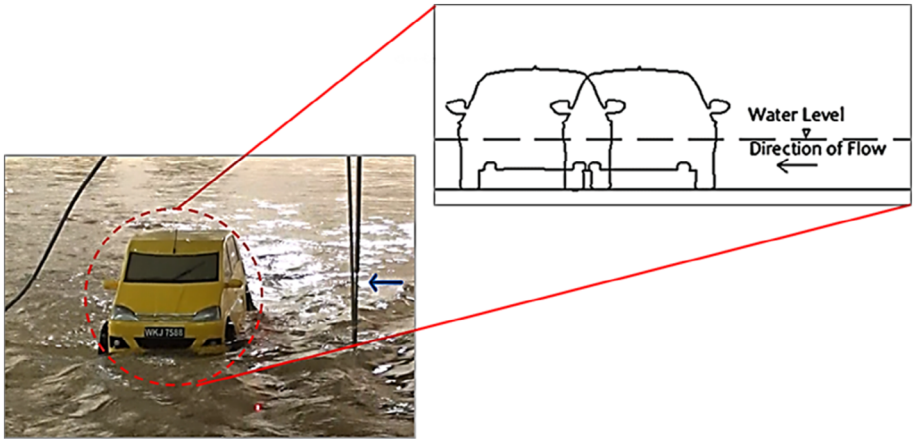


**FIGURE 15** Sliding instability

$$F_D > F_R + F_{RO} + F_{DV} \quad (24)$$

where, $F_D$ is the drag force at $D_1$, $F_R$ is the friction parallel to the direction of flow, $F_{RO}$ is the rolling friction in the direction of vehicle movement and $F_{DV}$ is the driving force.

Based on the given statements, Table 3 shows the floating instability computed through a comparison between $F_B$ and $W_T$. On the other hand, Table 4 shows sliding instability computed through a comparison between $F_D$, $F_R$, $F_{RO}$, and $F_{DV}$.

## 8 | VALIDATIONS

A comparison between empirical investigations (refer Figure 5) and theoretical validations through estimation of the hydrodynamic forces showed no noticeable difference for the instability threshold values. However, it has been noticed that at one point, the vehicle was found to be stable rather than sliding based on the theoretical assessment, as highlighted in Table 4 and further illustrated in Figure 16.

**TABLE 3** Floating instability computed through a comparison between $F_B$ and $W_T$ (8.628 N)

| No. | Water depth (m) | Buoyancy force, $F_B$ (N) | Floating instability ($F_B > W_T$) – Equation (23) |
|---|---|---|---|
| 1. | 0.041 | 7.48 | × |
| 2. | 0.047 | 9.70 | ✓ |
| 3. | 0.051 | 11.23 | ✓ |
| 4. | 0.053 | 12.01 | ✓ |
| 5. | 0.056 | 13.20 | ✓ |
| 6. | 0.067 | 18.22 | ✓ |
| 7. | 0.040 | 7.11 | × |
| 8. | 0.052 | 11.62 | ✓ |
| 9. | 0.058 | 14.01 | ✓ |
| 10. | 0.060 | 14.90 | ✓ |
| 11. | 0.067 | 18.22 | ✓ |
| 12. | 0.071 | 20.21 | ✓ |
| 13. | 0.073 | 21.19 | ✓ |
| 14. | 0.039 | 6.75 | × |
| 15. | 0.053 | 12.01 | ✓ |
| 16. | 0.065 | 17.22 | ✓ |
| 17. | 0.075 | 22.18 | ✓ |
| 18. | 0.081 | 25.11 | ✓ |
| 19. | 0.083 | 26.07 | ✓ |
| 20. | 0.040 | 7.11 | × |
| 21. | 0.047 | 9.70 | ✓ |
| 22. | 0.056 | 13.20 | ✓ |
| 23. | 0.065 | 17.22 | ✓ |
| 24. | 0.071 | 20.21 | ✓ |
| 25. | 0.075 | 22.18 | ✓ |
| 26. | 0.04 | 7.11 | × |
| 27. | 0.039 | 6.75 | × |
| 28. | 0.045 | 8.95 | ✓ |
| 29. | 0.051 | 11.23 | ✓ |
| 30. | 0.067 | 18.22 | ✓ |
| 31. | 0.071 | 20.21 | ✓ |
| 32. | 0.076 | 22.70 | ✓ |
| 33. | 0.038 | 6.38 | × |

(Continues)

**TABLE 3** (Continued)

| No. | Water depth (m) | Buoyancy force, $F_B$ (N) | Floating instability ($F_B > W_T$) – Equation (23) |
|---|---|---|---|
| 34. | 0.045 | 8.95 | ✓ |
| 35. | 0.057 | 13.60 | ✓ |
| 36. | 0.065 | 17.22 | ✓ |
| 37. | 0.076 | 22.70 | ✓ |
| 38. | 0.084 | 26.55 | ✓ |
| 39. | 0.089 | 28.91 | ✓ |
| 40. | 0.047 | 9.70 | ✓ |
| 41. | 0.051 | 11.23 | ✓ |
| 42. | 0.054 | 12.40 | ✓ |
| 43. | 0.056 | 13.20 | ✓ |
| 44. | 0.057 | 13.60 | ✓ |
| 45. | 0.060 | 14.90 | ✓ |
| 46. | 0.062 | 15.78 | ✓ |
| 47. | 0.052 | 11.62 | ✓ |
| 48. | 0.071 | 20.21 | ✓ |
| 49. | 0.081 | 25.11 | ✓ |
| 50. | 0.086 | 27.50 | ✓ |
| 51. | 0.087 | 27.97 | ✓ |
| 52. | 0.091 | 29.83 | ✓ |
| 53. | 0.038 | 6.38 | × |
| 54. | 0.047 | 9.70 | ✓ |
| 55. | 0.051 | 11.23 | ✓ |
| 56. | 0.067 | 18.22 | ✓ |
| 57. | 0.084 | 26.55 | ✓ |
| 58. | 0.095 | 31.62 | ✓ |
| 59. | 0.099 | 33.38 | ✓ |

**TABLE 4** Sliding instability computed through a comparison between $F_D$, $F_R$, $F_{RO}$ and $F_{DV}$

| No. | Water depth (m) | Flow velocity (m/s) | Drag force, $F_D$ (N) | Rolling friction, $F_{RO}$ (N) | Friction force, $F_R$ (N) | Driving force, $F_{DV}$ (N) | Sliding instability ($F_D > F_R + F_{RO} + F_{DV}$) – Equation (24) |
|---|---|---|---|---|---|---|---|
| 1. | 0.041 | 0.55 | 1.35 | 0.12 | 0.60 | 0.00023 | ✓ |
| 7. | 0.040 | 0.57 | 1.39 | 0.15 | 0.79 | 0.00085 | ✓ |
| 14. | 0.039 | 0.60 | 1.48 | 0.19 | 0.98 | 0.00461 | ✓ |
| 20. | 0.040 | 0.55 | 1.30 | 0.15 | 0.79 | 0.00087 | ✓ |
| 26. | 0.040 | 0.59 | 1.49 | 0.15 | 0.79 | 0.00047 | ✓ |
| 27. | 0.039 | 0.52 | 1.11 | 0.19 | 0.98 | 0.00049 | Stable |
| 33. | 0.038 | 0.61 | 1.46 | 0.23 | 1.17 | 0.00297 | ✓ |
| 53. | 0.038 | 0.60 | 1.41 | 0.23 | 1.17 | 0.00122 | ✓ |

The threshold points discussed earlier, while emphasising the experimental investigations concerning sliding instability, showed no stable conditions. However, from the theoretical perspective, it was found that at one date point, the vehicle was found to be stable rather than sliding. However, the other values agreed well with the

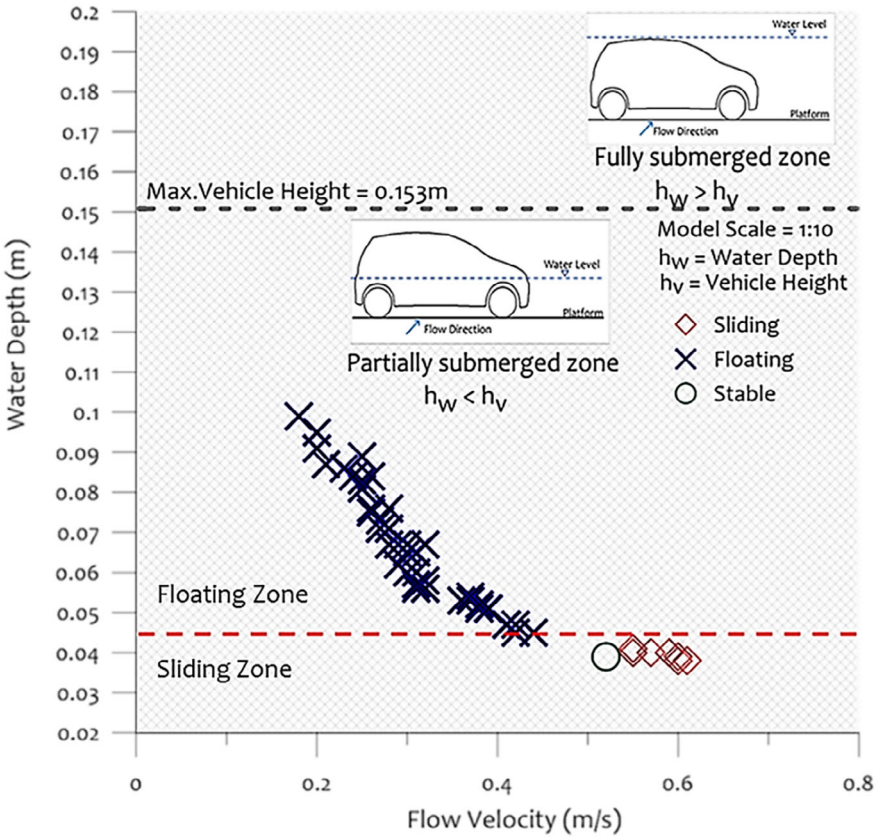


**FIGURE 16** Instability thresholds assessed through theoretical equations

experimental findings. Thus, in total, the percentage error between the experimental investigations and the theoretical analysis was found to be below 2%. Therefore, it can be concluded that the proposed approach has led to the estimation of the hydrodynamic impacts on flooded vehicles in an advanced way and this approach is applicable in analysing the partially submerged non-static vehicles attempting to cross subcritical flows on flat flooded roadways.

## 9 | INCIPIENT VELOCITY FORMULA

The mechanics-based incipient velocity formula required to cause sliding instability for non-stationary vehicles follows the mechanical theory of sliding equilibrium, which states that:

$$F_D > F_R + F_{RO} + F_{DV} \tag{25}$$

where, $F_D$ is the drag force at $D_1$, $F_R$ is the friction resistance perpendicular to the direction of incoming flow, $F_{RO}$ is the rolling friction and $F_{DV}$ is the driving force.

By substituting the values of $F_D$, $F_{RO}$, $F_R$ and $F_{DV}$ into Equation (25), the final proposed equation becomes:

$$\frac{1}{2}\rho C_D A_D v^2 = \frac{(W-F_b)\times b}{\sqrt{(r+b)(r-b)}} + (W-F_B)\times\mu + ma \tag{26}$$

Rearrangement of Equation (26) gives:

$$v = \sqrt{2\times\frac{(W-\rho gV)xb + \{(W-\rho gV)x\mu + ma\}.\sqrt{(r+b)(r-b)}}{\sqrt{(r+b)(r-b)}\times\rho C_D A_D}} \tag{27}$$

where, $v$ is the incipient velocity required to cause sliding instability, $W$ is the weight of vehicle in dry conditions, $\rho$ is the density of water, $g$ is the acceleration due to gravity, $V$ is the submerged volume of the vehicle, $\mu$ is the coefficient of frictional resistance on the tires (both parallel and opposite to the direction of incoming flow), $m$ is the mass of the vehicle (Equation (14)), a is the acceleration, $r$ is the radius of the tire, $b$ is the distance from the middle of the centre of the axle towards the tire no longer touching the ground, $C_D$ is the drag coefficient and $A_D$ is the submerged area projected normal to the flow.

To assess the prediction accuracy of the proposed formula, the instability thresholds (i.e., sliding instability) of a partially submerged vehicle were analysed. Figure 17 shows the linear regression using the least

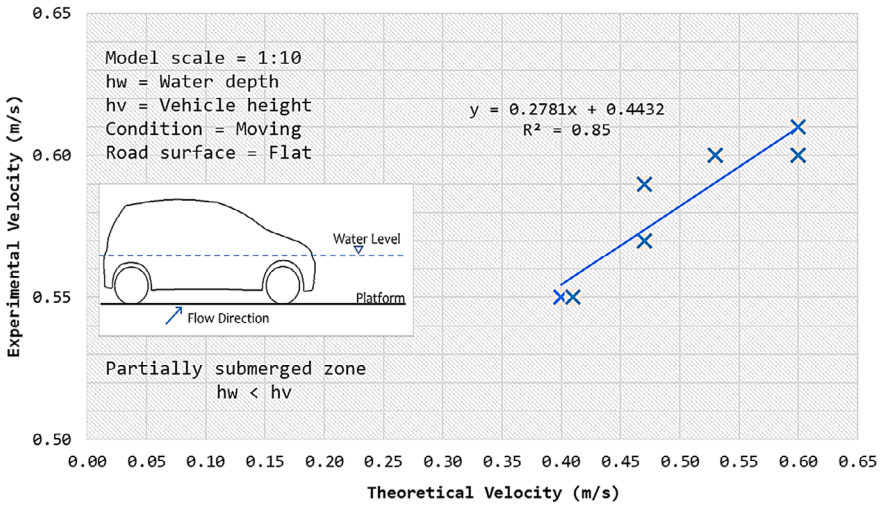


**FIGURE 17** Prediction accuracy of proposed formula for the incipient velocity

squares method by comparing the observed incipient velocities obtained through experimental investigations and the calculations attained from the derived formula (Equation (27)). The predicted velocities from the derived formula are in good agreement with the observed data for all points, with a correlation coefficient of 0.85. Therefore, the formula appears to be useful for estimating the incipient velocities for a prototype vehicle using Froude similarity.

## 10 | CONCLUSIONS

In the current approach, the hydrodynamic response of a partially submerged non-stationary vehicle crossing a flat flooded roadway under subcritical flow conditions was studied and an incipient velocity formula, based on the mechanical theory of sliding equilibrium, has been proposed. In this study a passenger car, namely a Perodua Viva (1:10), was used and its response towards the governing hydrodynamic forces caused by the flowing water at varying depths was investigated.

The main findings have highlighted: (a) an inverse variation between buoyancy and the drag force ($D_2$), and a positive relationship between the drag force ($D_1$), $F_R$ and $F_{RO}$ with respect to the Froude number, (b) drag influence at $D_2$, was nominal, due to the low flow velocity and a smaller submerged area, thus for subcritical flow conditions its impact can be disregarded for a small size passenger car, (c) the empirical value of the friction coefficient due to tire rotation, as well as being parallel to flow direction, was found to be 0.092 and 0.52, respectively, (d) the drag caused by air resistance was disregarded, due to the slow vehicle speed, (e) for all instability threshold points, the incipient velocity increased with a decrease in the flood water depth and vice versa, (f) an up-thrust force governed at water depths greater than, or equal to, 0.0457 m, whereas below this depth, the drag force dominated over the frictional and driving forces, initiating sliding failure, and lastly (g) predicted velocities from the derived formula were in good agreement with the observed data, with a correlation coefficient of $R^2 = 0.85$.

The outcomes provide a preliminary criterion of hazard level for non-stationary vehicles attempting to cross a flat flooded roadway. However, to ensure the practical application of the derived formula, a reliable assessment of drag and lift coefficients contributing to the incipient motion condition under different flow regimes needs to be conducted. Further, it is proposed that studies on the non-static cars should be performed on different roadway conditions in future, such as (a) inclined road – car moving uphill and downhill, (b) car moving straight but with different angles relative to flood flow, (c) car moving along a curve, in which case front wheels turn under different angles (in order to ensure that imaginary lines drawn through all wheels perpendicular to them cross each other at the same point), and are getting inclined as the angle of turning increases (in order to be approximately vertical when a car is curving at high speed) etc.

## ACKNOWLEDGEMENTS

This research was supported by Universiti Teknologi PETRONAS (UTP) Internal Grant URIF 0153AAG24 and the Technology Innovation Program (Grant No.: 10053121) funded by the Ministry of Trade, Industry & Energy (MI, Korea).

## DATA AVAILABILITY STATEMENT

N/A

## ORCID

*Syed Muzzamil Hussain Shah* https://orcid.org/0000-0003-0991-686X

*Eduardo Matínez-Gomariz* https://orcid.org/0000-0002-0189-0725


## REFERENCES


Abt, S. R., Wittier, R. J., Taylor, A., & Love, D. J. (1989). Human stability in a high flood hazard zone. *Journal of the American Water Resources Association*, *25*, 881–890.

Arrighi, C., Castelli, F., and Oumeraci, H. (2016). Effects of flow orientation on the onset of motion of flooded vehicles. Sustainable Hydraulics in the Era of Global Change, 837–841. doi: https://doi.org/10.1201/b21902-140.

Biezen, M. V. (2017). What is rolling friction. Ch 11: Friction, Mechanical Engineering. http://ilectureonline.com.

Bonham, A. J., & Hattersley, R. T. (1967). Low level causeways (Tech. Rep. No. 100). University of New South Wales, Water Research Laboratory.

Ejsmont, J. A., Ronowski, G., Świeczko-Żurek, B., & Sommer, S. (2017). Road texture influence on tyre rolling resistance. *Road Materials and Pavement Design*, *18*(1), 181–198.

Gordon, A. D. & Stone, P. B. (1973). *Car stability on road causeways* (WRL Technical Report No. 73/12). 5p + Appendices.

Gordon, A. D., & Stone, P. B. (1973). *Car stability on road floodways. National Capital Development Commission, Report no. 73/12*. Australia: Water Research Laboratory, University of New South Wales.

Keller, R. J., & Mitsch, B. F. (1993). *Safety aspects of design roadways as floodways (Research Report No. 69)*. Melbourne Australia: Urban Water Research Association of Australia.

Martínez-Gomariz, E., Gómez, M., Russo, B., & Djordjevi, C. S. (2016). Stability criteria for flooded vehicles: A state-of-the-art review. *Journal of Flood Risk Management*, *11*(S2), S817–S826.

Martínez-Gomariz, E., Gómez, M., Russo, B., & Djordjevi, C. S. (2017). A new experiments-based methodology to define the stability threshold for any vehicle exposed to flooding. *Urban Water Journal*, *14*(9), 930–939.

Martínez-Gomariz, E., Gómez, M., Russo, B., Sánchez, P., & Montes, J. (2019). Methodology for the damage assessment of vehicles exposed to flooding in urban areas. *Journal of Flood Risk Management*, e12475.*12*

Moore, K., & Power, R. (2002). Safe buffer distances for offstream earth dams. *Australasian Journal of Water Resources*, *6*(1), 1–15.

Royston, A. (2013). *Forces and motion*. Essential Physical Science Raintree, UK: Heinemann Educational Books.

Russo, B., Velasco, M., & Suñer, D. (2013). Flood hazard assessment considering climate changeimpacts-application to Barcelona case study using a 1D/2D detailed coupled model. In International Conference on Flood Resilience: Experiences in Asia and Europe, Exeter, UK.

Russo, B., Gómez, M., & Macchione, F. (2013). Pedestrian hazard criteria for flooded urban areas. *Natural Hazards*, *69*(1), 251–265.

Sanyal, J., & Lu, X. X. (2006). GIS-based flood hazard mapping at different administrative scales: A case study in Gangetic West Bengal, India. *Singapore Journal of Tropical Geography*, *27*(2), 207–220.

Shah, S. M. H., Mustaffa, Z., & Yusof, K. W. (2018). Experimental studies on the threshold of vehicle instability in floodwaters. *Jurnal Teknologi*, *80*(5), 25–36.

Shah, S. M. H., Mustaffa, Z., Yusof, K. W., & Nor, M. F. M. (2018). Influence of forces on vehicle's instability in floodwaters. *Ain Shams Engineering Journal*, *9*(4), 3245–3258.

Shah, S. M. H., Mustaffa, Z., Matínez-Gomariz, E., Kim, D. K., & Yusof, K. W. (2019). Criterion of vehicle instability in floodwaters: Past, present and future. *International Journal of River Basin Management*, 1–23. https://doi.org/10.1080/15715124.2019.1566240.

Shand, T. D., Cox, R. J., Blacka, M. J., & Smith, G. P. (2011). Australian rainfall and runoff revision project 10: Appropriate safety criteria for vehicles – Literature review (Stage 2 Report).

Shu, C., Xia, J., Falconer, R. A., & Lin, B. (2011). Incipient velocity for partiallysubmerged vehicles in floodwaters. *Journal of Hydraulic Research*, *49*(6), 709–717.

Smith, G. P., Modra, B. D., & Felder, S. (2019). Full-scale testing of stability curves for vehicles in flood waters. *Journal of Flood Risk Management*, *12*(suppl 2), e12527.

Te-Chow, V. (1959). *Open channel hydraulics*. New York: McGraw-Hill Book Company, Inc.

Teo, F. Y. (2010). Study of the hydrodynamic processes of rivers and floodplains with obstructions. Ph.D. Thesis, Cardiff School of Engineering, Cardiff University, UK.

Teo, F. Y., Falconer, R. A., Lin, B., & Xia, J. (2012). Investigations of hazard risks relating to vehicles moving in flood. *Journal of Water Resources Management*, *1*(1), 52–66.

Teo, F. Y., Falconer, R. A., & Lin, B. (2012). Experimental studies on the interaction between vehicles and floodplain flows. *International Journal of River Basin Management*, *10*(2), 149–160.

Toda, K., Ishigaki, T., & Ozaki, T. (2013). Experiment study on floating car in flooding. In International conference on flood resilience: Experiences in Asia and Europe. Exeter, UK.

Van Drie, R., Simon, M., & Schymitzek, I. (2008). HAZARD:-is there a better definition? & impact of not accounting for buildings! In 48th Annual Floodplain Management Authorities Conference, New South Wales, Australia.

Xia, J., Teo, F. Y., Lin, B., & Falconer, R. A. (2010). Formula of incipient velocity for flooded vehicles. *Natural Hazards*, *58*(1), 1–14.

Xia, J., Falconer, R. A., Xiao, X., & Wang, Y. (2013). Criterion of vehicle stability in floodwaters based on theoretical and experimental studies. *Natural Hazards*, *70*, 1619–1630.

Xia, J., Falconer, R. A., Wang, Y., & Xiao, X. (2014). New criterion for the stability of a human body in floodwaters. *Journal of Hydraulic Research*, *52*, 93–104.



**How to cite this article:** Shah SMH, Mustaffa Z, Matínez-Gomariz E, Yusof KW. Hydrodynamic effect on non-stationary vehicles at varying Froude numbers under subcritical flows on flat roadways. *J Flood Risk Management*. 2020;e12657. https://doi.org/10.1111/jfr3.12657